2018

# Crack Healing in Cementitious Mortars Using Enzyme-Induced Carbonate Precipitation: Quantification Based on Fracture Response

Akash Dakhane

Sumanta Das

***See next page for additional authors***

**Authors**
Akash Dakhane, Sumanta Das, Hannah Hansen, Sean O'Donnell, Farouq Hanoon, Aimee Rushton, Carlos Perla, and Narayanan Neithalath

# Crack Healing in Cementitious Mortars using Enzyme Induced Carbonate Precipitation (EICP): Quantification Based on Fracture Response

**Akash Dakhane[*], Sumanta Das[†,‡] ,Hannah Hansen[§], Sean O'Donnell[**], Farouq Hanoon[††], Aimee Rushton[‡‡], Carlos Perla[§§], Narayanan Neithalath[***],**

**ABSTRACT**

A non-microbial means of carbonate precipitation to heal cracks in concrete is evaluated in this paper. Enzyme induced carbonate precipitation (EICP) that relies on plant-derived urease enzyme is used to catalyze the reaction between calcium chloride and urea to precipitate calcium carbonate. The faster rate of carbonate precipitation and the absence of microbes makes this method attractive to surface applications for crack healing of concrete. Notched mortar beams, where pre-cracking is induced, are subjected to EICP solutions with different $CaCl_2$ concentrations and a fixed molar ratio of urea-to-$CaCl_2$ of 1.2. X-ray diffraction and thermal analysis of samples collected from the vicinity of the notch clearly demonstrate the presence of calcium carbonate in the cracks. A flexural strength enhancement of about 33% is observed for mortars treated with an EICP solution made using 0.5 M $CaCl_2$ as compared to the mortars that are just moist cured, while the fracture toughness doubled. The strength and fracture parameters (fracture toughness, and critical crack tip opening displacement) scale well with the carbonate content. Digital image correlation (DIC) is used to quantify the reduction in crack extension after the beams are treated with the EICP solution.

**Keywords:** Crack healing; Carbonate precipitation; Fracture; Strain energy release; Digital image correlation

[*] Graduate student, School of Sustainable Engineering and the Built Environment, Arizona State University, Tempe AZ, USA
[†] Assistant Professor, Civil and Environmental Engineering, University of Rhode Island, Kingston RI, USA
[‡] Corresponding Author, E-mail: sumanta_das@uri.edu; Phone: +1-401-874-5637, Fax: +1-401-874-2786
[§] Undergraduate student, School of Sustainable Engineering and the Built Environment, Arizona State University, Tempe AZ, USA
[**] Staff Engineer, Geosyntec Consultants, 10211 Wincopin Circle, Floor 4, Columbia, MD, USA
[††] NSF REU Student, Center for Bio-mediated and Bio-inspired Geotechnics, Arizona State University, Tempe AZ, USA
[‡‡] High school research student, Center for Bio-mediated and Bio-inspired Geotechnics, Arizona State University, Tempe AZ, USA
[§§] NSF RET Participant, Center for Bio-mediated and Bio-inspired Geotechnics, Arizona State University, Tempe AZ, USA
[***] Professor, School of Sustainable Engineering and the Built Environment, Arizona State University, Tempe AZ, USA

## 1.0 INTRODUCTION

Cracking is among the most important factors that compromise the durability of concrete structures. The ingress of deleterious agents through cracks result in corrosion of reinforcing steel, and other chemically induced durability problems, which further accelerate cracking, and exacerbate deterioration. Several strategies are used to obtain self-sealing and self-healing of cracks in concrete, including the use of epoxy-based materials, acrylic resins, and silicone-based polymers [1–3]. In addition to crack sealing, methods of crack healing also have been investigated in great detail. In a humid environment, concrete is known to exhibit autogenous healing through the hydration of unhydrated cement, even though this process is very slow and applicable only to very narrow cracks [4]. When water and $CO_2$ are available inside the crack, healing could occur through the carbonation of leached calcium hydroxide [5–8]. Other possible self-healing mechanisms have also been described [9–13]. A microencapsulation approach that incorporates a healing agent into a capsule that ruptures when confronted by a crack, and polymerizes to seal the crack, has been well reported for both concretes and other composites [14,15]. Silica shell microcapsules containing functionalized silica nano-particles have also been studied to obtain smart self-healing concrete [16]. While microcapsules are frequently applied to obtained crack healing in polymers and composites, for concrete, most often larger capsules are embedded to release the healing agent.

Bio-mediated self-healing of concrete has been extensively investigated in the recent past. In general, a bacteria-based self-healing system consists of alkali resistant spore-forming bacteria and a substrate that is added to concrete during the mixing process. The dormant spores could be activated by water and oxygen in the event of a crack, and the organic substrate (i.e., urea) is metabolized by the active bacteria [17,18]. The basic premise behind microbially induced carbonate precipitation (MICP) is that the enzymatic hydrolysis of urea catalyzed by the microbially produced urease enzyme, in the presence of calcium ions, results in the precipitation of calcium carbonate [19–22]. The precipitated carbonates seal the cracks and enhance concrete properties. The bacterial spores and organic compounds are typically encapsulated (in polymeric shells, silica shells, lightweight aggregates etc.) in order to immobilize the bacteria and protect them before being incorporated into the concrete matrix [23,24]. MICP has also been established to be advantageous for several other engineering applications including cementation of soil to protect against liquefaction [25,26], and fugitive dust control [27]. Several studies have evaluated the microstructure of healed concrete and expounded the potential improvements in durability of concrete through MICP [17,24,28–33]. Non-ureolytic bacteria combined with an organic calcium source as a two-component healing system for concrete has also been proposed [17,34].

While MICP relies on microbes to generate the urease enzyme, this study directly employs a plant-derived urease enzyme to catalyze the necessary reactions that induce carbonate precipitation in cracks in mortars, thus eliminating the need to use bacteria. Enzyme induced carbonate precipitation (EICP) is reported to have several advantages over MICP such as: (i) improved efficiency since it does not consume or compete for urea, (ii) water soluble free enzyme allows for easier in-situ application for crack control, (iii) smaller size of the solubilized urease enzyme than the microbially generated one, enabling penetration into smaller cracks, and (iv) short life of urease activity that enables faster production of carbonates and enzyme degradation that eliminates long-term impacts to concrete [35]. The rapid carbonate precipitation induced by the EICP process makes it well-suited for surface treatment of cracks in concrete, and thus attractive for infrastructural management agencies. The influence of different EICP solutions and treatment durations on the crack healing of mortars is investigated in this work. The EICP solutions if developed appropriately, can be encapsulated and used as self-healing material in concrete. Notched mortar beams are subjected to pre-cracking before subjecting them to EICP. The fracture toughness and strain energy release rates of the healed beams are evaluated to understand and quantify the efficiency of EICP in crack-healing of concrete structures. Digital image correlation (DIC) is employed to determine crack propagation rates in these beams.

## 2.0 EXPERIMENTAL PROGRAM

### 2.1 Materials and Mixtures

The cementitious mortars used in this study were prepared using a commercially available ordinary portland cement (OPC) conforming to ASTM C 150, and quartz sand. A mass-based water-to-cement ratio (w/c) of 0.40 (corresponding to a volumetric w/c of 1.26), and a sand volume fraction of 50% was used. The quartz sand had a mean particle size of 0.6 mm. The mortar mixtures were cast in 330 mm x 76 mm x 25 mm beam molds. A 19 mm notch was cut using a diamond saw at the center span of the beams (corresponding to a notch depth-to-beam depth ratio of 0.25). All the specimens were cured in moist conditions (RH > 98%) at a temperature of 23 ± 2$^{o}$C for a period of 28 days.

### 2.2 EICP Solution Formulation

The EICP solution used in this study was formulated based on [35]. The molar ratio of urea to $CaCl_2$ was maintained at 1.2:1. Two different $CaCl_2$ concentrations of 0.5 M and 1.0 M were used. The enzyme solution was designed to obtain a concentration of 1.0 g/l urease (Sigma Aldrich Type III Jack Bean Urease). Laboratory grade $CaCl_2$ and urea were used for the experiments. While $CaCl_2$ is used here to show the effectiveness of EICP process, a suitable alternative of calcium chloride, such as calcium hydroxide, could

be used to avoid durability concerns posed by chlorides. Non-fat dry milk was used as a stabilizer because it has stable glycoproteins that coordinate (not bond) with the enzyme and do not interfere with the enzyme's active site. The EICP solutions were prepared by mixing two different stock solutions. The first solution consisted of 2.0 g/l low activity (200 units/g) urease enzyme and 4.0g/l of stabilizer, and the second solution consisted of 2.0 M $CaCl_2$ and 2.4 M urea. The stock solutions were mixed in a 1:1 ratio to generate a high concentration treatment solution (termed HC). The first and second stock solutions were mixed in a 2:1 ratio along with 1 part DI water to generate a low concentration treatment solution (termed LC). The solution and treatment details are shown in Table 1.

Table 1: EICP treatment details on pre-cracked beams

| Specimen ID | EICP solution information | | | | Treatment after pre-cracking |
|---|---|---|---|---|---|
| | $CaCl_2$ conc. (M) | Urea conc. (M) | Urease conc. (g/l) | Stabilizer (Nonfat dry milk) (g/L) | |
| Control | NA | | | | 14 days (moist curing) |
| LC-7 | 0.5 | 0.6 | 1.0 | 2.0 | 7 days (EICP solution) |
| LC-14 | 0.5 | 0.6 | | | 14 days (EICP solution) |
| HC-7 | 1.0 | 1.2 | | | 7 days (EICP solution) |

### 2.3 Strength and Fracture Response Testing

The flexural strength of the notched beams was determined using standard center-point loading as per ASTM C293/293M-10, after 28 days of moist curing. Based on the obtained flexural strengths, a total of 24 beams were loaded in three-point bending to a CMOD of 0.032 mm (approximately 95% of the peak load) in a closed-loop testing machine with the crack-mouth opening displacement (CMOD), measured using a clip gauge, acting as the feedback signal. This process was intended to create a controlled single crack above the notch in these beams. All the beams had similar crack tip opening displacements (CTOD) and crack lengths above the notch, which were around 20 µm and 12 mm respectively. After this pre-cracking procedure, the beams were subjected to the following treatment procedure: (i) six beams were returned to the moist-curing chamber, and (iii) three sets of six beams each were subjected to EICP solutions. Two sets of beams were subjected to the LC solution for 7 days and 14 days respectively, and the remaining set subjected to the HC solution for 7 days, as shown in Table 1. The sides of the notch were sealed, and the notches were filled with the respective EICP solutions. Since the EICP process is a fast reaction, stock solutions were mixed immediately prior to treating the beams. The beams were treated every day for the desired duration to enable continuous carbonate precipitation. The experimental procedure is schematically described in Figure 1.

After the respective treatment durations, the beams were again subjected to the three-point bending tests under CMOD control (Figure 2(a)). The tests were terminated at a CMOD of 0.20 mm. Both monotonic (one loading and unloading cycle), and cyclic (multiple loading and unloading cycles) tests were carried out. Digital image correlation (DIC) was used to determine the crack propagation features in the monotonic testing regime. The cyclic regime was used to determine the fracture parameters (e.g., fracture toughness) and compliance-based fracture resistance curves (R-curves).

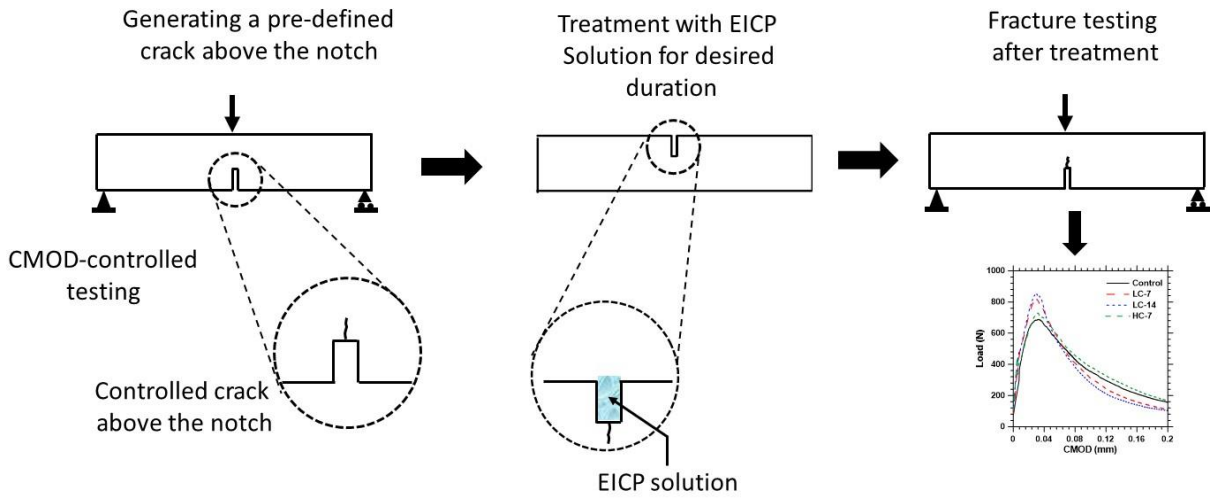


Figure 1: Schematic of the EICP treatment and fracture testing procedure

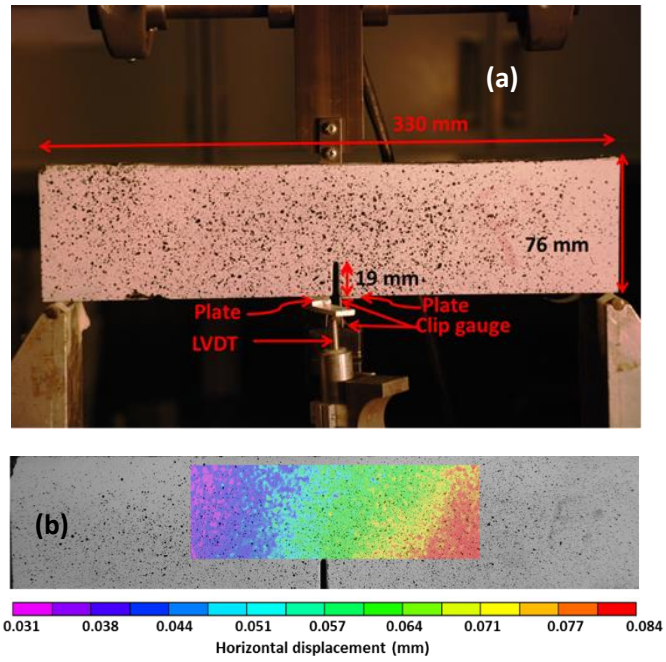

Figure 2: (a) Experimental set up for three-point bending test on notched beams under CMOD-controlled mode, (b) horizontal (*u*) displacement field from DIC in the pre-peak region.

DIC is a non-contact optical method that provides full-field surface displacements of the sample using digital images taken at different time intervals during the mechanical testing. The beam surface was speckled with random patterns to provide adequate contrast for image correlation (See Figure 2(a)). A Charge-Coupled Device (CCD) camera recorded images every 5 seconds during the monotonic testing regime. A rectangular area of approximately 120 mm x 60 mm above the notch was imaged. After termination of the test, the digital images were post-processed. The correlation between the subset of images corresponding to different locations in the load-CMOD plot was determined in order to calculate the displacement fields (Figure 2(b)) using VIC-2D software$^{TM}$ (Correlated Solutions). The requisite mathematical formulations can be found in [36,37]. The horizontal (u) and vertical (v) displacement fields were obtained through the minimization of the correlation coefficient [38].

### 2.4 Identification and Quantification of Carbonate Precipitation

X-Ray Diffraction (XRD) and thermal analysis were used to ascertain the enhancement in the amount of carbonates precipitated in the crack through the EICP treatments. Small chunks were removed from the vicinity of the notch in the beams which were exposed to EICP treatment. These chunks were powdered to prepare them for XRD and thermal analysis.

XRD was carried out using a Siemens D-5000 diffractometer in a $\theta$-$\theta$ configuration using Cu-K$\alpha$ radiation ($\lambda$=1.54 Å). The samples were scanned on a rotating stage between 10$^o$ and 70$^o$ (2$\theta$) in a continuous mode with a step scan of 0.02$^o$ and step rate of 0.5/second. High-Score Xpert Analysis software was used for phase identification. Thermal analysis was carried out using a simultaneous thermal analyzer (Perkin Elmer STA 6000) in a nitrogen environment, at a gas flow rate of 20 ml/s. The samples were heated from ambient temperature to 995°C at a heating rate of 15°C/min. At least three replicate samples were used for thermal analysis.

## 3.0 RESULTS AND DISCUSSIONS

### 3.1 Quantification of Carbonate Precipitation

Figure 3 shows the XRD spectra of powdered samples from the control beam as well as the different EICP solution treated beams. The peaks corresponding to 2$\theta$ of 23.02$^o$, 29.41$^o$, and 39.40$^o$ represent the calcite

polymorph of calcium carbonate. It can be noticed that the peak intensities are higher in the samples treated with EICP solutions after pre-cracking, than in the control sample which was moist cured after pre-cracking. This is an indication of carbonate precipitation in the cracks, resulting in its healing. The LC-14 sample (treated for 14 days with a solution containing 0.5 M $CaCl_2$, 0.6 M urea, and 0.5 g/l urease) shows the highest carbonate peak intensity. The major peaks occurring at 2$\theta$ values of 18.09°, 34.09°, and 47.12° are attributable to portlandite (calcium hydroxide), the major crystalline component in hydrated portland cement systems.

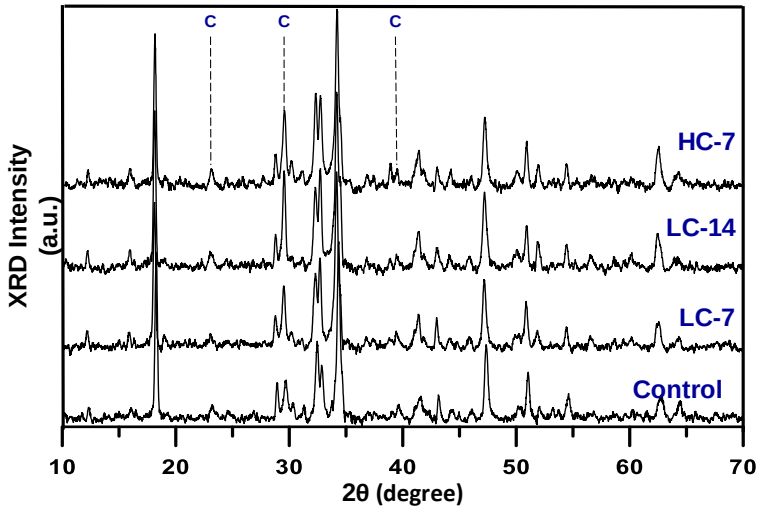


Figure 3: XRD spectra of the control and EICP solution treated samples. “C” indicates calcium carbonate

Figure 4(a) shows the thermogravimetric (TG) and differential TG (DTG) curves for the untreated and EICP solution treated samples after the respective treatment durations. Thermal analysis tests on cement-based materials typically illustrate three distinct peaks attributable to: (i) loss of evaporable water and chemically bound water in C-S-H and ettringite, in the range of 110-130°C, (ii) dehydroxylization of calcium hydroxide around 450°C, and (iii) decarbonation of calcium carbonate, in the range of 650-800°C, as can be noted from Figure 4(a). It can be noticed that the peak in the 110-130°C range is higher for the EICP solution treated samples. This is possibly the effect of chlorides from the treatment solution that acts to accelerate the hydration of unhydrated cement in the vicinity of the crack. Note that the treatment solution was applied only along the crack, and samples for thermal analysis were sourced from the same location. For the treated samples, an additional peak in the DTG curve is observed around 175°C, which likely comes from the decomposition of excess or precipitated calcium chloride from the treatment solution [39]. The calcium hydroxide contents in the treated samples are lower than that in the control sample. This can be explained by the dissolution of calcium ions from the calcium hydroxide present in

the hydrated products, aided by the treatment solution that initially has a lower pH than the concrete pore solution. The calcium ions that are dissociated from calcium hydroxide, as well as those from calcium chloride which is a part of the treatment solution, reacts with the carbonate ions to form calcium carbonate. This is evident from the carbonate peaks in the DTG curves. For the control (untreated) sample, only one dominant peak corresponding to calcium carbonate is observed, around 720°C, while an additional, more pronounced carbonate dissociation peak around 800°C is observed for the treated samples. The thermal dissociation of calcium carbonate is influenced by the grain size [40]; the carbonate species resulting from atmospheric carbonation (generally of calcium hydroxide in the cement pastes) dissociates much before the carbonates precipitated from the EICP reaction, which explains the presence of multiple carbonate peaks in the DTG curves.

The peak corresponding to carbonate decomposition was used in this study to quantify the amount of carbonates precipitated through the EICP treatment. Figure 4(b) shows the amount of calcium carbonate present in the vicinity of the notch in the control and treated pastes. Some of this carbonate can be attributed to atmospheric carbonation. A significant amount of calcium carbonate is precipitated in the treated mortars, resulting in crack healing, which has the potential to improve the mechanical properties, as will be discussed in the forthcoming sections. The LC-14 sample shows the highest amount of calcium carbonate, which is in line with the XRD spectra shown in Figure 3. Based on carbonate quantification as a function of EICP solution composition and treatment duration, it seems that a longer duration of treatment using a lower concentration solution is a beneficial option. The use of a higher concentration solution is found to result in slightly more carbonate precipitation over 7 days than the lower concentration solution, but the difference is not very significant. This is likely because the efficiency of urease is inhibited by high calcium chloride concentrations [35].

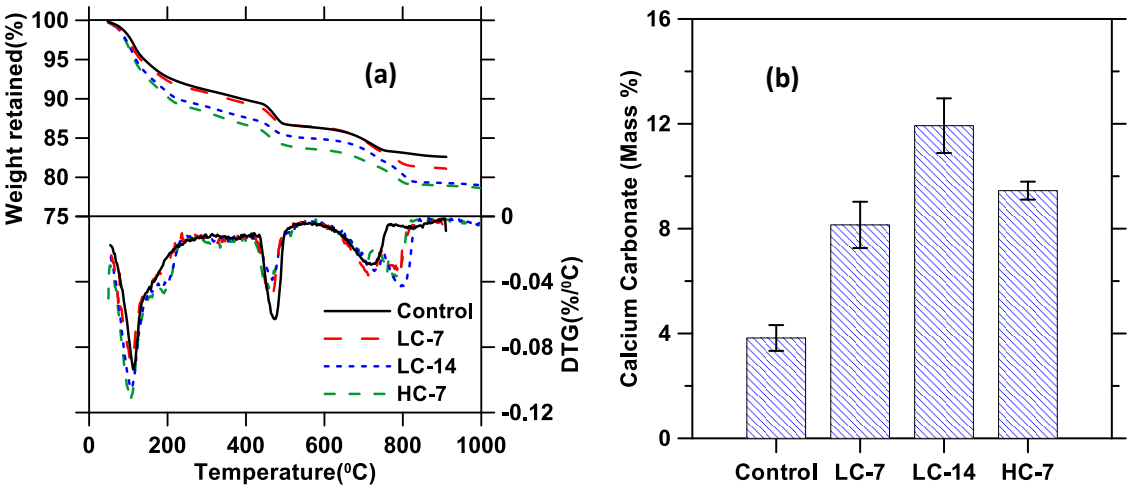

Figure 4: (a) TG and DTG curves of the control and EICP solution treated samples, (b) calcium carbonate contents in the samples as a function of the treatment type/duration

### 3.2 Mechanical Response of the Treated Mortars: Quantification of Crack Healing Efficiency

#### 3.2.1 Strength enhancement

The mechanical response of the beams treated with EICP solutions were determined to quantify the beneficial impacts of carbonate precipitation in the induced crack. The treated beams were loaded in three-point bending to obtain load-CMOD plots as shown in Figure 5(a), from which the flexural strengths (Figure 5(b)) were obtained. It is seen that the flexural strengths of the treated beams are higher than that of the control mortar which was moist-cured. The strength increase is attributed to carbonate precipitation, which partly (or fully) heals the induced crack above the notch. The relative increase in strength as compared to the control mortar is in line with the amount of carbonates precipitated (Figure 4(b)), with the LC-14 sample showing the highest strength. The crack healing efficiency of EICP treatment, as evidenced by the strength increase, provides options to develop surface application strategies to cracked concrete structures to enhance their mechanical and durability properties.

A magnified view of the load-CMOD response of the beams in the region of approximately 25% to 50% of the peak load is shown in the inset of Figure 5(a). Because of the presence of the pre-existing crack, and the absence of any crack-healing, the control specimen shows a lower initial load, while the treated specimens show higher loads because of the carbonate precipitation in the cracks. However, around a CMOD of 5 to 6 µm, there is a sudden drop in the load of the treated specimens, after which load again increases. The drop can be attributed to the breaking/failure of the calcite in the cracks, after which the specimen begins to take more load. Note that the drop is much larger for the HC-7 specimen, which is likely the result of differences in calcite morphology, as discussed in a later section. At a CMOD of around 10 µm, the loads in the control and HC-7 specimens become almost identical and this trend is followed for the entire load-CMOD response.

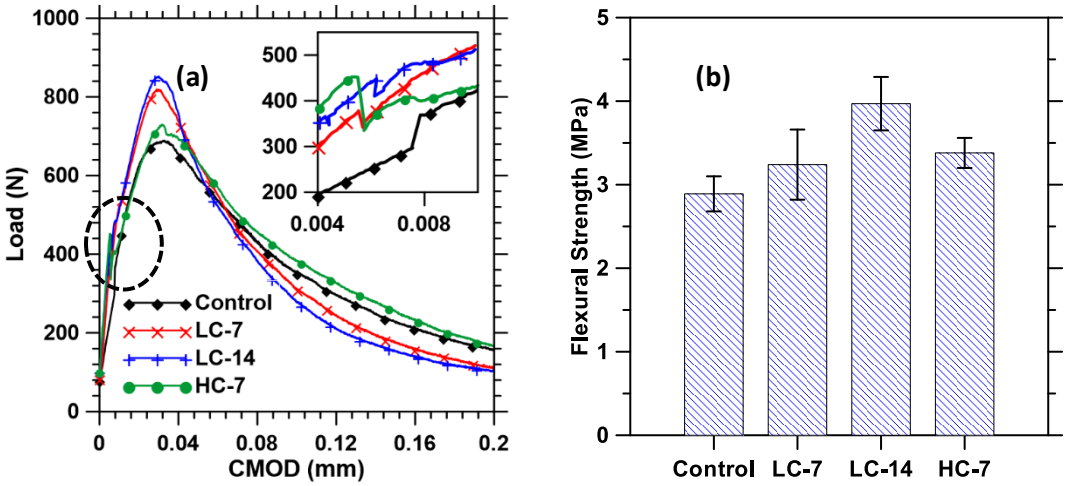


Figure 5: (a) Load-CMOD response under monotonic loading, and (b) post-treatment flexural strengths of the mortars (notched beam test). The data in the marked circle is magnified in the inset in (a).

### 3.2.2 Fracture parameters ($K_{IC}$, $CTOD_c$, and $G_R$)

The fracture parameters considered in this study for the control and treated mortars are the critical stress intensity factor or the fracture toughness ($K_{IC}$), critical crack tip opening displacement ($CTOD_c$), and the strain energy release rate ($G_R$). $K_{IC}$ and $CTOD_c$ were evaluated using the two-parameter fracture model (TPFM). TPFM uses loading and unloading compliances (from one loading and unloading cycle), peak load, specimen and notch geometry, and a geometry correction factor to determine the values of $K_{IC}$ and $CTOD_c$ [41,42]. Multiple loading-unloading cycles were used to determine $G_R$. The non-linear response in the pre-peak region in a notched beam (notch depth $a_0$) is accounted for through the consideration of an effective elastic material containing a crack length of $a_{eff}$ ($a_{eff} > a_0$). Representative load-CMOD responses under several loading-unloading cycles, used to determine the TPFM parameters and $G_R$ are shown in Figure 6. The pre-peak slopes are higher for the treated samples, indicating a higher elastic modulus, attributable to crack healing. The LC-14 sample shows the highest peak strength and elastic modulus because of the higher carbonate content. It is also important to note that the post-peak drop is more significant for the treated samples, plausibly indicating debonding of carbonate crystals from the mortar and/or breakage of the carbonate crystals.

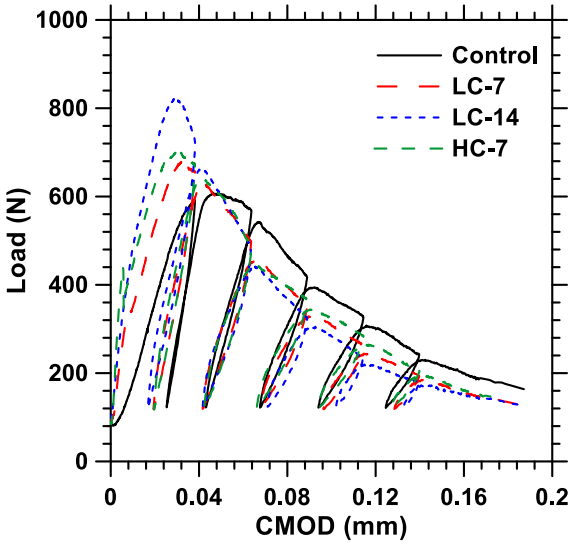


Figure 6: Load-CMOD relationship under multiple loading-unloading cycles to determine the fracture parameters

Figures 7(a) and (b) depict $K_{IC}$ and $CTOD_c$ respectively of the treated and untreated mortar samples, extracted using TPFM. $K_{IC}$, which is an elastically equivalent fracture toughness, is one the most important fracture parameters of cement-based materials. Similar to the flexural strength results, the fracture toughness and $CTOD_c$ values are also higher for the treated samples, with the LC-14 sample showing the highest improvement. Note that TPFM uses peak load in the calculation of $K_{IC}$, and that is reflected in the values shown in Figure 7(a). Carbonate precipitation fills the cracks, thereby not only enhancing the strength of the mortar, but also making the crack path more tortuous. Moreover, calcium carbonate is softer than the cement hydration products, aiding in energy dissipation. Both these aspects contribute to the enhancement of $K_{IC}$ of the treated mortars. Energy is also dissipated in breaking the bonds between the precipitates and the mortar, which also has the potential to increase the fracture toughness. Treatment with EICP solution also likely results in the precipitation of carbonates in small pores adjacent to the notch, thereby resulting in further reaction product densification and pore size refinement, which also could contribute to improving the strength and toughness [42,43]. The enhancement in toughness scales with the carbonate content as shown in Figure 7(c).

$CTOD_c$ represents the crack tip opening beyond which unstable crack propagation begins. The carbonate precipitation in the cracks increases the $CTOD_c$ values, and thus delays the start of unstable crack

propagation in the treated mortars. The trend, once again, relates well to the carbonate content as shown in Figure 7(c). In fact, the beneficial increase in $CTOD_c$ due to EICP is larger than the corresponding increase for $K_{IC}$, which is indicative of the energy dissipation provided by the carbonates precipitated in and around the crack.

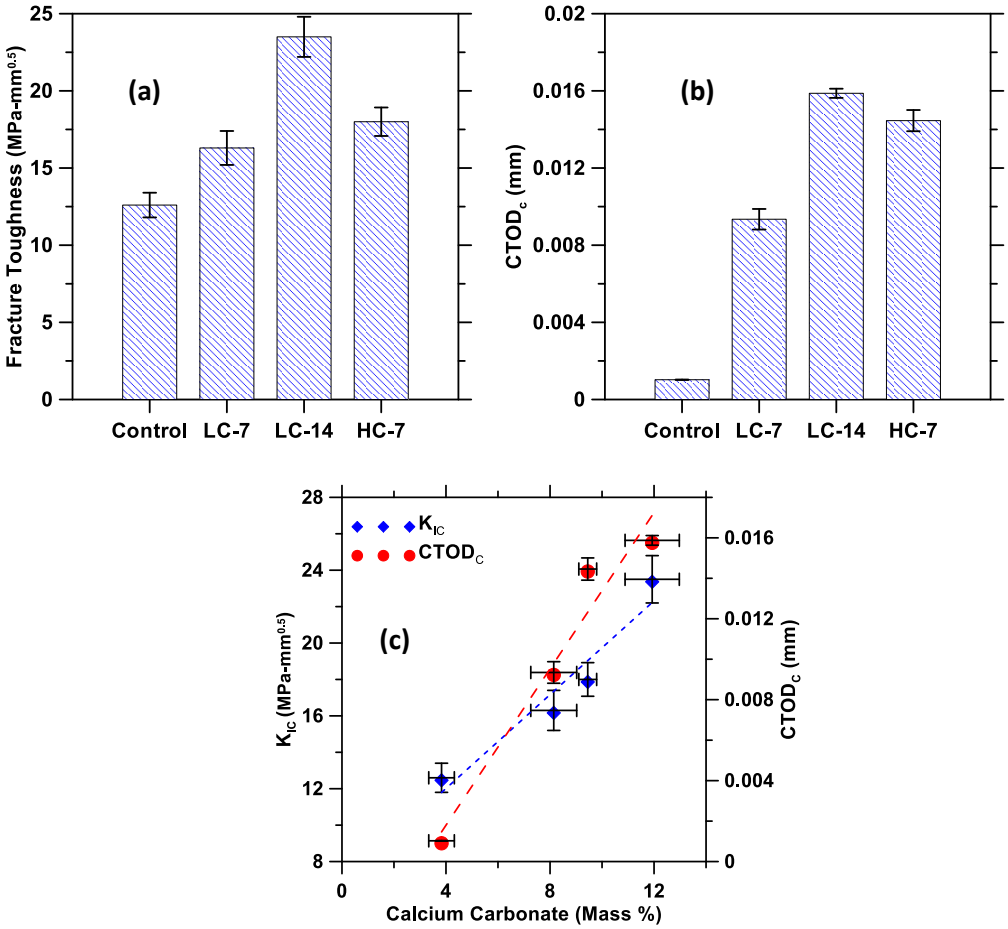


Figure 7: (a) Fracture toughness, and (b) $CTOD_c$ of the control and treated mortars, (c) relationship between the carbonate contents and $K_{IC}$ or $CTOD_c$(error bars indicate standard deviation)

Resistance curves (R-curves) employ multiple loading-unloading cycles (Figure 6) from the closed-loop CMOD controlled testing of notched beams to better elucidate the crack growth process in cementitious materials [44,45]. R-curves are envelopes of strain energy release rates and they represent the strain energy release rate ($G_R$) as a function of crack extension. The fact that stable crack propagation increases the compliance of the specimen is used to extract the R-curves. $G_R$ is determined as shown in Equation 1:

$$G_R = \frac{P^2}{2t}\frac{\partial C}{\partial a} + \frac{P}{2t}\frac{\partial (CMOD_{inelastic})}{\partial a} \quad (1)$$

The first term is the elastic component and the second, the inelastic component of strain energy. Here, P is the applied load, C is the unloading compliance, t is the thickness of the specimen and a is the crack length. $CMOD_{inelastic}$ is the residual CMOD when the sample is unloaded, which can be obtained from Figure 6. The elastic component is calculated using the rate of change of the unloading compliance with crack length, and corresponds to the energy release rate due to incremental crack growth. The inelastic component considers the rate of change of inelastic CMOD with crack length, and corresponds to permanent deformation caused due to crack opening. Both the rate components in Equation 1 are obtained by differentiating polynomial curve fits of compliance-crack length and inelastic CMOD-crack length relationships. Effective crack length ($a_0+\Delta a$) is obtained by solving a non-linear equation that considers the beam span and geometry, unloading compliance, and the elastic modulus [46]. Crack extension ($\Delta a$) is extracted from each of the unloading compliances from the cyclic load – CMOD curves in Figure 6.

Figure 8 shows the crack growth resistance curves for the control and treated mortars. In general, R-curves of cement-based materials comprise of a rising portion (indicating the formation of fracture process zone, the region of non-linearity at the tip of the crack) and a plateau region (indicating steady-state crack growth). It can be seen that the strain energy release rates of all the mortars are higher than that of the control mortar in the steady-state crack growth region. Thus it can be safely stated that the treated mortars require a higher strain energy for a given crack extension than the control mortar in this regime, because of the presence of energy dissipating mechanisms as discussed earlier. These trends are consistent with those of $K_{IC}$ and $CTOD_c$. However, in the low crack extension stage (i.e., in the pre-peak region), the HC-7 mortar shows lower $G_R$ than all the other mortars. A previous work on EICP in test tubes showed that lower concentration solutions are capable of producing calcite crystals with a more uniform size distribution. This is attributed to the slower mineral precipitation [35]. With higher concentration solutions, the precipitation is rapid and non-uniform crystals, visually appearing as agglomerations of small crystals, are formed. Note that the calcite contents are rather invariant between LC-7 and HC-7 samples as noticed from Figure 5(b). It is plausible that the presence of non-uniform, agglomerated crystals in the crack (even though the carbonate volume fraction remains roughly the same) dissociate quickly in the event of a crack driving force, forcing large crack extensions at lower strain energies. It was shown in Figure 5(a) that the drop in load for the HC-7 mortar was higher than those in LC-7 and LC-14 mortars, substantiating this deduction. However, the volume of calcite filling the cracks is roughly the

same irrespective of the solution concentration (i.e., between LC-7 and HC-7 in Figure 4(b)); thus after dissociation of the grains, the energy balance becomes favorable for steady-state crack growth in this case also. The bulk fracture parameters $K_{IC}$ and $CTOD_c$ are not able to capture this behavior since they are averaged global quantities. Thus the R-curves provide a more refined understanding of the micro-scale crack propagation response, and help explain the material behavior better. This also helps to choose the appropriate treatment methodology for crack healing.

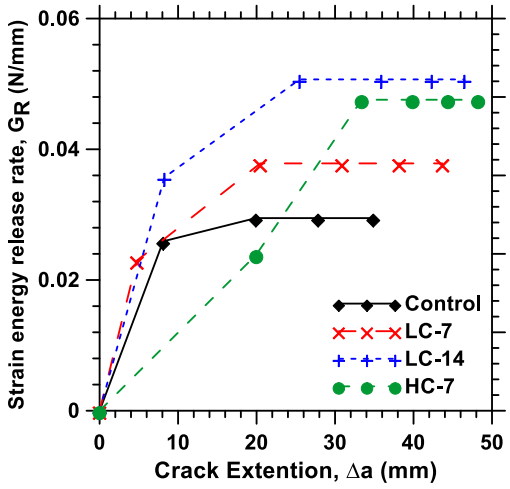


Figure 8: Crack growth resistance as a function of crack extension for the control and treated mortars

### 3.3 Crack Propagation in the Treated Beams

Crack propagation is significantly influenced by the microstructure of the material. The deposition of calcite in the crack influences the propagation of the crack under loading. Since the control mortar is not subjected to any crack healing treatment, cracks propagate faster under a smaller load, as evidenced by the fracture toughness and strain energy release rates shown earlier. In this section, the localized response at the tip of the crack is quantified using digital image correlation (DIC) to bring out the effectiveness of EICP in controlling crack lengths.

The 2D displacement fields obtained from DIC for the control and LC-14 mortar specimens are shown in Figures 9(a) and (b) respectively. These two samples alone are shown here to bring out the contrast between the control and best-performing EICP-treated samples. The images correspond to a CMOD of 0.04 mm, which corresponds to 95% of the peak load in the post-peak regime as can be noted from Figure 5(a). This is the region of unstable crack propagation. In both figures, the displacement jump is visible at the tip of the notch. The crack extension ($\Delta a$) can be measured based on the extent of the displacement

jump along the Y-direction at the notch tip (x = 0), whereas the crack tip opening displacement (CTOD) can be measured from the displacement jump at {x=0; y=0} [42]. Figures 9(c) and (d) show the corresponding 3D surface plots of the horizontal (u) displacements obtained from DIC for the control and LC-14 mortar samples. A displacement jump of 0.005 mm was set as a threshold limit to qualify the displacement jump as contributing to the extension of the crack. At a CMOD of 0.04 mm, the crack extension is significantly lower for the EICP-treated sample as compared to the untreated control sample. Note that at this CMOD, the treated sample also carries a higher load (Figure 5(a)); yet the crack extension is lower. These results reinforce the results reported earlier in this paper and attests to the efficiency of EICP-based crack healing method.

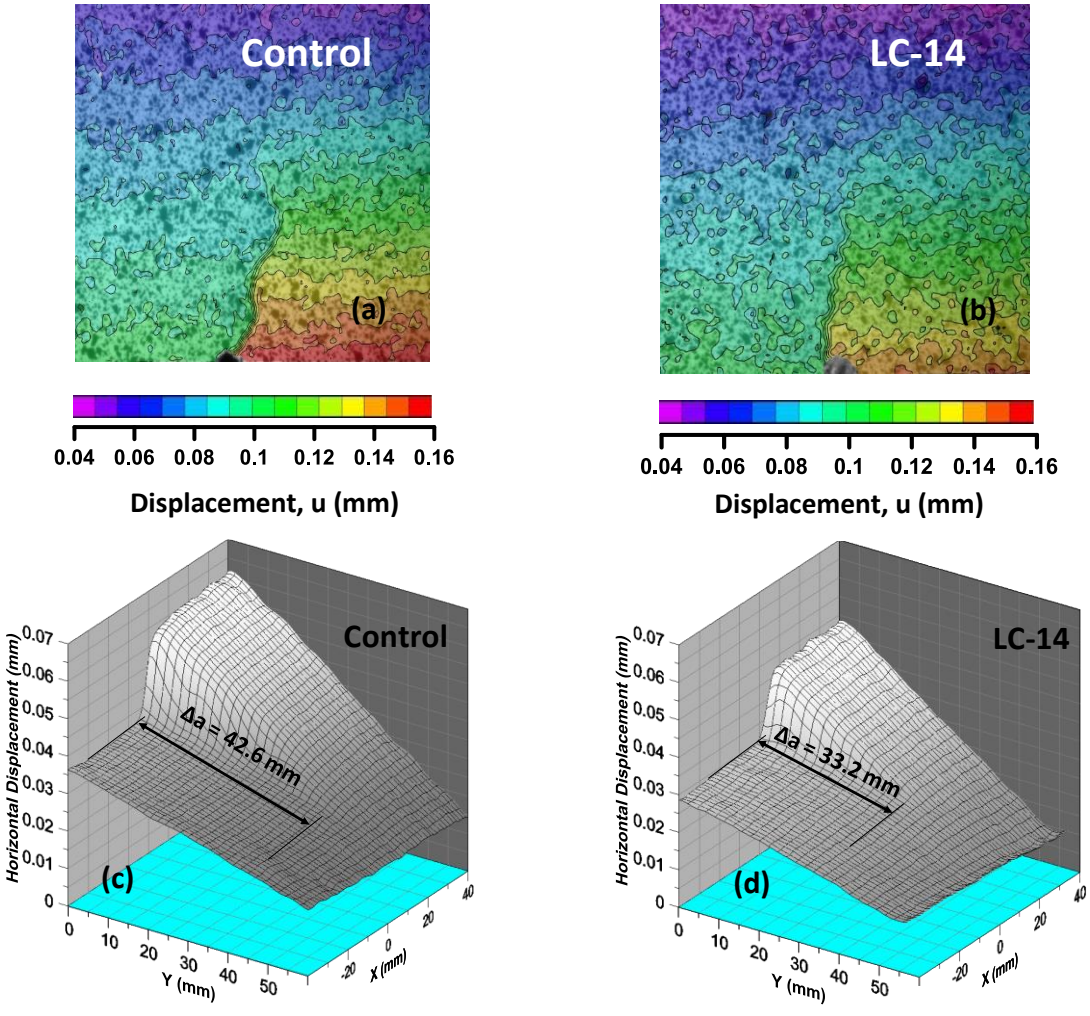


Figure 9: (a) and (b): 2D horizontal (u) displacement fields at 0.04 mm CMOD for the control and LC-14 mortars, and (c) and (d): 3D plots of displacement field to determine crack extension and CTOD

In order to shed more light into the relative healing efficiency of different treated samples as compared to the untreated one, rate of crack extension with respect to change in CMOD ($\Delta a/\Delta CMOD$) is plotted at as a function of CMOD in Figure 10. The $\Delta a$ values corresponding to all the CMOD values were determined from DIC as explained earlier. The crack extension rate is shown only for CMOD values beyond about 60% to 70% of the peak load since before this load, crack extension is rather minimal. Due to the existence of an unhealed crack, a significant amount of energy is utilized in extending the crack in the control sample at relatively lower loads as can be noticed from Figure 10. The EICP-treated samples exhibit significantly lower crack extension rate, especially at loads before and close to the peak (CMOD ≤ 0.04 mm) as compared to the control mortar, attributable to carbonate precipitation that heals the crack and thus provides higher strain energy release rates (Figure 8). The crack extension rates are the lowest for the LC-14 sample, which is in line with the amount of carbonate precipitated, and the other fracture characteristics determined earlier. Beyond the peak (which is higher for the treated mortars), the rate of crack extension is rather invariant for all the samples because energy has already been expended in driving the crack through the healed locations.

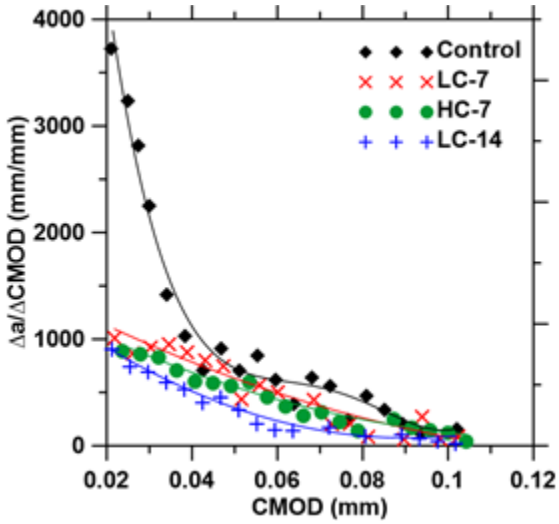


Figure 10: Crack extension rates of the control and EICP-treated mortars as a function of CMOD

**4.0 SUMMARY AND CONCLUSIONS**

The efficiency of enzyme induced carbonate precipitation (EICP) as a crack healing methodology for concrete was evaluated in this study. Plant-derived urease enzyme was used to catalyze the reaction between calcium chloride and urea to precipitate calcium carbonate in the cracks. This non-microbial method of carbonate precipitation has several advantages over microbial induced carbonate precipitation

(MICP). Two different $CaCl_2$ concentrations at the same molar ratio of urea-to-$CaCl_2$ (of 1.2) were used for two different treatment durations in this study. Notched mortar beams were pre-cracked using a crack mouth opening displacement (CMOD) controlled test procedure, and then subjected to either moist curing or the EICP treatment.

XRD and thermal analysis studies conclusively demonstrated the presence of calcium carbonate in the cracks of the mortar beams after EICP treatment. The carbonate contents trended as: LC-7 < HC-7 < LC-14, which also matched well with the trends in the flexural strengths of the treated samples. Detailed fracture studies were carried out on the mortars to elucidate the effectiveness of the treatment methods. Both the parameters of the two-parameter fracture model (TPFM), viz., fracture toughness ($K_{IC}$), and critical crack mouth opening displacement ($CTOD_c$) were found to increase linearly with increase in carbonate content. The treated mortars were found to require a higher strain energy for a given crack extension than the control mortar, because of the presence of energy dissipating mechanisms introduced in the cracks by the precipitated calcite crystals. Digital image correlation clearly showed that the crack extension at or close to the peak load, as well as the rate of crack extension in the pre-peak region, were significantly reduced through EICP. The experimental studies conclusively showed the benefits of EICP in healing concrete cracks. The EICP method, where the calcite precipitation is rather quick, can be applied as a surface treatment strategy to heal cracks in concrete infrastructural elements.

## 5.0 ACKNOWLEDGEMENTS

The authors gratefully acknowledge support for this study from the U.S. National Science Foundation (NSF) under the Engineering Research Centers (ERC) program, grant no. EEC-1449501. Hannah Hansen acknowledges the Fulton Undergraduate Research Initiative (FURI) program at ASU for support. Farooq Hanoon acknowledges the NSF REU program and Carlos Perla acknowledges the NSF RET program for the support. Any opinions or positions expressed in this paper are those of the authors only, and do not reflect the opinions or positions of the NSF.

## 6.0 REFERENCES

[1] H.X.D. Lee, H.S. Wong, N.R. Buenfeld, Self-sealing of cracks in concrete using superabsorbent polymers, Cem. Concr. Res. 79 (2016) 194–208.

[2] J. Feiteira, E. Gruyaert, N. De Belie, Self-healing of moving cracks in concrete by means of encapsulated polymer precursors, Constr. Build. Mater. 102, Part 1 (2016) 671–678.

[3] M. Araújo, S. Van Vlierberghe, J. Feiteira, G.-J. Graulus, K. Van Tittelboom, J.C. Martins, P. Dubruel, N. De Belie, Cross-linkable polyethers as healing/sealing agents for self-healing of cementitious materials, Mater. Des. 98 (2016) 215–222.

[4] Z. Lv, H. Chen, Modeling of self-healing efficiency for cracks due to unhydrated cement nuclei in hardened cement paste, Procedia Eng. 27 (2012) 281–290.
[5] Y. Yang, E.-H. Yang, V.C. Li, Autogenous healing of engineered cementitious composites at early age, Cem. Concr. Res. 41 (2011) 176–183.
[6] K. Van Tittelboom, E. Gruyaert, H. Rahier, N. De Belie, Influence of mix composition on the extent of autogenous crack healing by continued hydration or calcium carbonate formation, Constr. Build. Mater. 37 (2012) 349–359.
[7] H. Ranaivomanana, J. Verdier, A. Sellier, X. Bourbon, Sealing process induced by carbonation of localized cracks in cementitious materials, Cem. Concr. Compos. 37 (2013) 37–46.
[8] A. Talaiekhozan, A. Keyvanfar, A. Shafaghat, R. Andalib, M.A. Majid, M.A. Fulazzaky, R.M. Zin, C.T. Lee, M.W. Hussin, N. Hamzah, others, A review of self-healing concrete research development, J. Environ. Treat. Tech. 2 (2014) 1–11.
[9] M. Wu, B. Johannesson, M. Geiker, A review: Self-healing in cementitious materials and engineered cementitious composite as a self-healing material, Constr. Build. Mater. 28 (2012) 571–583.
[10] B. Pang, Z. Zhou, P. Hou, P. Du, L. Zhang, H. Xu, Autogenous and engineered healing mechanisms of carbonated steel slag aggregate in concrete, Constr. Build. Mater. 107 (2016) 191–202.
[11] K. Van Tittelboom, N. De Belie, Self-Healing in Cementitious Materials—A Review, Materials. 6 (2013) 2182–2217.
[12] Z. Lv, D. Chen, Overview of recent work on self-healing in cementitious materials, Mater. Constr. 64 (2014) e034.
[13] L. Ferrara, V. Krelani, F. Moretti, On the use of crystalline admixtures in cement based construction materials: from porosity reducers to promoters of self healing, Smart Mater. Struct. 25 (2016) 84002.
[14] S.R. White, N.R. Sottos, P.H. Geubelle, J.S. Moore, M.R. Kessler, S.R. Sriram, E.N. Brown, S. Viswanathan, Autonomic healing of polymer composites, Nature. 409 (2001) 794–797.
[15] B. Boh, B. Šumiga, Microencapsulation technology and its applications in building construction materials Tehnologija mikrokapsuliranja in njena uporaba v gradbenih materialih, RMZ–Materials Geoenvironment. 55 (2008) 329–344.
[16] G. Perez, E. Erkizia, J.J. Gaitero, I. Kaltzakorta, I. Jiménez, A. Guerrero, Synthesis and characterization of epoxy encapsulating silica microcapsules and amine functionalized silica nanoparticles for development of an innovative self-healing concrete, Mater. Chem. Phys. 165 (2015) 39–48.
[17] M. Luo, C. Qian, Influences of bacteria-based self-healing agents on cementitious materials hydration kinetics and compressive strength, Constr. Build. Mater. 121 (2016) 659–663.
[18] J.Y. Wang, H. Soens, W. Verstraete, N. De Belie, Self-healing concrete by use of microencapsulated bacterial spores, Cem. Concr. Res. 56 (2014) 139–152.
[19] S. Stocks-Fischer, J.K. Galinat, S.S. Bang, Microbiological precipitation of CaCO3, Soil Biol. Biochem. 31 (1999) 1563–1571.
[20] R. Wang, C. Qian, J. Wang, Bio-deposition of a calcite layer on cement-based materials by brushing with agar-immobilised bacteria, Adv. Cem. Res. 23 (2011) 185–192.
[21] T. Zhu, M. Dittrich, Carbonate Precipitation through Microbial Activities in Natural Environment, and Their Potential in Biotechnology: A Review, Front. Bioeng. Biotechnol. 4 (2016).
[22] E. Schlangen, S. Sangadji, Addressing Infrastructure Durability and Sustainability by Self Healing Mechanisms - Recent Advances in Self Healing Concrete and Asphalt, Procedia Eng. 54 (2013) 39–57.
[23] V. Wiktor, H.M. Jonkers, Quantification of crack-healing in novel bacteria-based self-healing concrete, Cem. Concr. Compos. 33 (2011) 763–770.
[24] E. Tziviloglou, V. Wiktor, H.M. Jonkers, E. Schlangen, Bacteria-based self-healing concrete to increase liquid tightness of cracks, Constr. Build. Mater. 122 (2016) 118–125.

[25] Carbonate Mineral Precipitation for Soil Improvement through Microbial Denitrification, in: Geo-Front. 2011 (accessed February 26, 2017).
[26] J.T. DeJong, M.B. Fritzges, K. Nüsslein, Microbially induced cementation to control sand response to undrained shear, J. Geotech. Geoenvironmental Eng. 132 (2006) 1381–1392.
[27] N. Hamdan, E. Kavazanjian, Enzyme-induced carbonate mineral precipitation for fugitive dust control, Géotechnique. 66 (2016) 546–555.
[28] S.S. Bang, J.J. Lippert, U. Yerra, S. Mulukutla, V. Ramakrishnan, Microbial calcite, a bio-based smart nanomaterial in concrete remediation, Int. J. Smart Nano Mater. 1 (2010) 28–39.
[29] W. De Muynck, K. Cox, N. De Belie, W. Verstraete, Bacterial carbonate precipitation as an alternative surface treatment for concrete, Constr. Build. Mater. 22 (2008) 875–885.
[30] W. De Muynck, D. Debrouwer, N. De Belie, W. Verstraete, Bacterial carbonate precipitation improves the durability of cementitious materials, Cem. Concr. Res. 38 (2008) 1005–1014.
[31] K. Van Tittelboom, N. De Belie, W. De Muynck, W. Verstraete, Use of bacteria to repair cracks in concrete, Cem. Concr. Res. 40 (2010) 157–166.
[32] V. Achal, A. Mukerjee, M. Sudhakara Reddy, Biogenic treatment improves the durability and remediates the cracks of concrete structures, Constr. Build. Mater. 48 (2013) 1–5.
[33] F. Pacheco-Torgal, J.A. Labrincha, Biotech cementitious materials: some aspects of an innovative approach for concrete with enhanced durability, Constr. Build. Mater. 40 (2013) 1136–1141.
[34] H.M. Jonkers, A. Thijssen, G. Muyzer, O. Copuroglu, E. Schlangen, Application of bacteria as self-healing agent for the development of sustainable concrete, Ecol. Eng. 36 (2010) 230–235.
[35] N. Hamdan, Applications of Enzyme Induced Carbonate Precipitation (EICP) for Soil Improvement, Arizona State University, 2015. https://repository.asu.edu/items/27573 (accessed February 26, 2017).
[36] S. Roux, J. Réthoré, F. Hild, Digital image correlation and fracture: an advanced technique for estimating stress intensity factors of 2D and 3D cracks, J. Phys. Appl. Phys. 42 (2009) 214004.
[37] C. Greiner, T. Merz, D. Braun, A. Codrignani, F. Magagnato, Optimum dimple diameter for friction reduction with laser surface texturing: the effect of velocity gradient, Surf. Topogr. Metrol. Prop. 3 (2015) 44001.
[38] J.R. Yates, M. Zanganeh, Y.H. Tai, Quantifying crack tip displacement fields with DIC, Eng. Fract. Mech. 77 (2010) 2063–2076.
[39] G. Fraissler, M. Jöller, T. Brunner, I. Obernberger, Influence of dry and humid gaseous atmosphere on the thermal decomposition of calcium chloride and its impact on the remove of heavy metals by chlorination, Chem. Eng. Process. Process Intensif. 48 (2009) 380–388.
[40] G. Villain, M. Thiery, G. Platret, Measurement methods of carbonation profiles in concrete: Thermogravimetry, chemical analysis and gammadensimetry, Cem. Concr. Res. 37 (2007) 1182–1192.
[41] Y. Jenq, S. Shah, Two Parameter Fracture Model for Concrete, J. Eng. Mech. 111 (1985) 1227–1241.
[42] S. Das, M. Aguayo, V. Dey, R. Kachala, B. Mobasher, G. Sant, N. Neithalath, The fracture response of blended formulations containing limestone powder: Evaluations using two-parameter fracture model and digital image correlation, Cem. Concr. Compos. 53 (2014) 316–326.
[43] M. D'Orazio, S. Lenci, L. Graziani, Relationship between fracture toughness and porosity of clay brick panels used in ventilated façades: Initial investigation, Eng. Fract. Mech. 116 (2014) 108–121.
[44] C. Ouyang, B. Mobasher, S. P. Shah., An r-curve approach for fracture of quasi-brittle materials, Eng. Fract. Mech. 37 (1990) 901–913.
[45] M. Wecharatana, S.P. Shah, A model for predicting fracture resistance of fiber reinforced concrete, Cem. Concr. Res. 13 (1983) 819–829.
[46] B. Mobasher, Mechanics of fiber and textile reinforced cement composites, CRC Press, 2011.